Antidepressants act by binding to the cholesterol-interaction site at TRKB neurotrophin receptor

Authors:

Plinio C Casarotto[1], Mykhailo Girych[2], Senem M Fred[1], Rafael Moliner[1], Giray Enkavi[2], Caroline Biojone[1], Cecilia Cannarozzo[1], Cecilia A Brunello[1], Anna Steinzeig[1], Frederike Winkel[1], Sudarshan Patil[3], Stefan Vestring[4], Tsvetan Serchov[5], Liina Laukkanen[1], Iseline Cardon[6], Hanna Antila[1,7], Tomasz Rog[2], Clive R Bramham[3], Claus Normann[4], Sari E Lauri[1,8], Ilpo Vattulainen[2,9], Eero Castrén[1]*

1. Neuroscience Center - HILIFE, University of Helsinki, Finland.
2. Department of Physics, University of Helsinki, Finland.
3. Department of Biomedicine and KG Jebsen Center for Research on Neuropsychiatric Disorders, University of Bergen, Norway.
4. Center for Neuromodulation, Department of Psychiatry and Psychotherapy, Medical Center, Faculty of Medicine, University of Freiburg, Germany.
5. Department of Stereotactic and Functional Neurosurgery, Laboratory of Stereotaxy and Interventional Neuroscience, Medical Center – University of Freiburg, Faculty of Medicine, University of Freiburg, Germany.
6. Brain Master Program, Faculty of Science, Aix-Marseille Université, Marseille, France.
7. Department of Neuroscience, Perelman School of Medicine, University of Pennsylvania, PA, USA.
8. Molecular and Integrative Biosciences Research Program, University of Helsinki, Finland.
9. Computational Physics Laboratory, Tampere University, Finland.

* corresponding author:

Eero Castren. eero.castren@helsinki.fi

Abstract

It is unclear how binding of antidepressant drugs to their targets gives rise to the clinical antidepressant effect. We found that both typical and fast-acting antidepressants bind to a cholesterol interaction motif in the BDNF receptor TRKB, a known mediator of neuronal plasticity and antidepressant responses. Cholesterol stabilized a cross-shaped configuration of TRKB transmembrane domain dimers and prolonged TRKB cell surface expression and activation by BDNF. Mutation of the TRKB cholesterol interaction site or cholesterol depletion by pravastatin impaired BDNF-mediated plasticity and cellular and behavioral responses to antidepressants *in vitro* and *in vivo*. We suggest that binding to and facilitation of TRKB activity is the common mechanism for antidepressant action, and propose a framework for how molecular effects of antidepressants are translated into clinical mood recovery.

Introduction

Several targets for antidepressant drug action were identified but it is not clear how these targets are translated into mechanisms for the clinical effect. Classical antidepressants increase the synaptic neurotransmitter levels (mainly serotonin and noradrenaline) by inhibition of reuptake or metabolism (*1*), while the rapid antidepressant effect of ketamine is attributed to inhibition of NMDA receptors (*2*, *3*). However, the low affinity of 2R,6R-hydroxynorketamine (RR-HNK), a ketamine metabolite with antidepressant-like activity, to NMDA receptors has called such mechanism into question (*4*, *5*). Therefore, it is not clear whether there is a common mechanism behind the antidepressant effect.

Essentially all antidepressants, including ketamine and RR-HNK, increase the expression of brain-derived neurotrophic factor (BDNF) and activate BDNF signaling through Neurotrophin Tyrosine Kinase Receptor 2 (TRKB) (*6*–*8*). Blocking TRKB signaling prevents the antidepressant-like effects in rodents (*4*, *5*, *7*–*10*). BDNF signaling through TRKB is a critical mediator of activity-dependent synaptic plasticity (*11*–*14*). The drug-induced BDNF-TRKB signaling reactivates a juvenile-like state of plasticity in the adult brain, which has been suggested to underlie the effects of antidepressant treatments on mood (*15*).

BDNF signaling is bidirectionally linked to brain cholesterol metabolism. BDNF, acting through TRKB, promotes production of cholesterol in neurons (*16*, *17*) and cholesterol regulates TRKB signaling (*18*, *19*). Cholesterol is essential for neuronal maturation and proper synaptic transmission (*20*, *21*). Since cholesterol does not pass the blood-brain barrier, neurons are dependent on cholesterol synthesized locally mostly by astrocytes (*22*). Synaptic cholesterol levels are low during the embryonic and early postnatal life but strongly increase during the 3rd postnatal week in mice (*23*), coincident with the increase in BDNF expression and appearance of antidepressants effects on TRKB (*24*). Many antidepressants interact with phospholipids (*25*, *26*) and accumulate to cholesterol-rich membrane microdomains, such as lipid rafts (*27*, *28*). These data prompted us to investigate the potential interactions between TRKB, cholesterol and antidepressants.

Cholesterol interacts with TRKB and promotes its activity and mobility

Bioinformatic mining revealed a region in TRKB transmembrane (TM) region that fulfils the criteria for inverted cholesterol recognition and alignment consensus (CARC) motif (*29*). This motif is specific to TRKB and not present in other TRK receptors (figure 1A). In primary cortical neurons (E18, DIV8-10), cholesterol at 20μM enhanced the effects of BDNF on TRKB phosphorylation (pTRKB), but at higher concentrations (50-100μM), cholesterol suppressed the effects of BDNF (figure 1B,C). The effects of BDNF on TRKB-PLC-γ1 interaction (figure 1D), as well as neurite branching (figure S1F), were prevented by prior treatment with pravastatin (1μM/3d), an inhibitor of cholesterol synthesis, as previously reported (*18*). Cholesterol-induced enhancement in TRKB:PLC-γ1 interaction was also blocked by cholesterol-sequestering agent beta-cyclodextrin (βCDX 2mM) (figure 1E). Cholesterol increased TRKB surface expression and TRKB:PLC-γ1 interaction in TRKB-expressing fibroblasts, but not in TRKA-expressing cells (figure S1A-E). A higher concentration of pravastatin (2μM/5d) reduced survival of cultured cortical neurons and this effect is attenuated by exogenous cholesterol (20μM), but not by BDNF (figure S2A,B), indicating that the effects of pravastatin are mediated through inhibition of cholesterol synthesis.

Many antidepressant drugs are cationic amphipathic molecules that interact with phospholipids (*25*, *26*) and accumulate to lipid rafts (*27*, *28*). We found that several antidepressants mimicked the effects of cholesterol and enhanced TRKB and PLC-γ1 interaction in primary cortical neurons, and, as for cholesterol, this effect was blocked by βCDX (figure 1E-I). Furthermore, fluoxetine increased the surface expression of TRKB in cortical neurons, and this effect was also prevented by βCDX (figure 1J). As noted above, higher doses of cholesterol (50μM) blunted the effects of BDNF on pTRKB, however, in the presence of fluoxetine (10μM), the effects of BDNF on pTRKB were partially recovered (figure 1K,L), suggesting that fluoxetine exerts a permissive effect on BDNF-induced activation of TRKB even under higher concentrations of cholesterol.

A

UniProt ID	aa res	transmembrane region sequence
Q3UFB7 (TRKA)	416-446	ETPFG***VSVAVGLAVSAALFLSALLLV***LNKCG
P15209 (TRKB)	425-458	SNREH***LSVYAVVVIASVVGFCLLVMLLLL***KLARH
Q6VNS1 (TRKC)	425-458	PEEDT***FGVSIAVGLAAFACVLLVVLFIMI***NKYGR

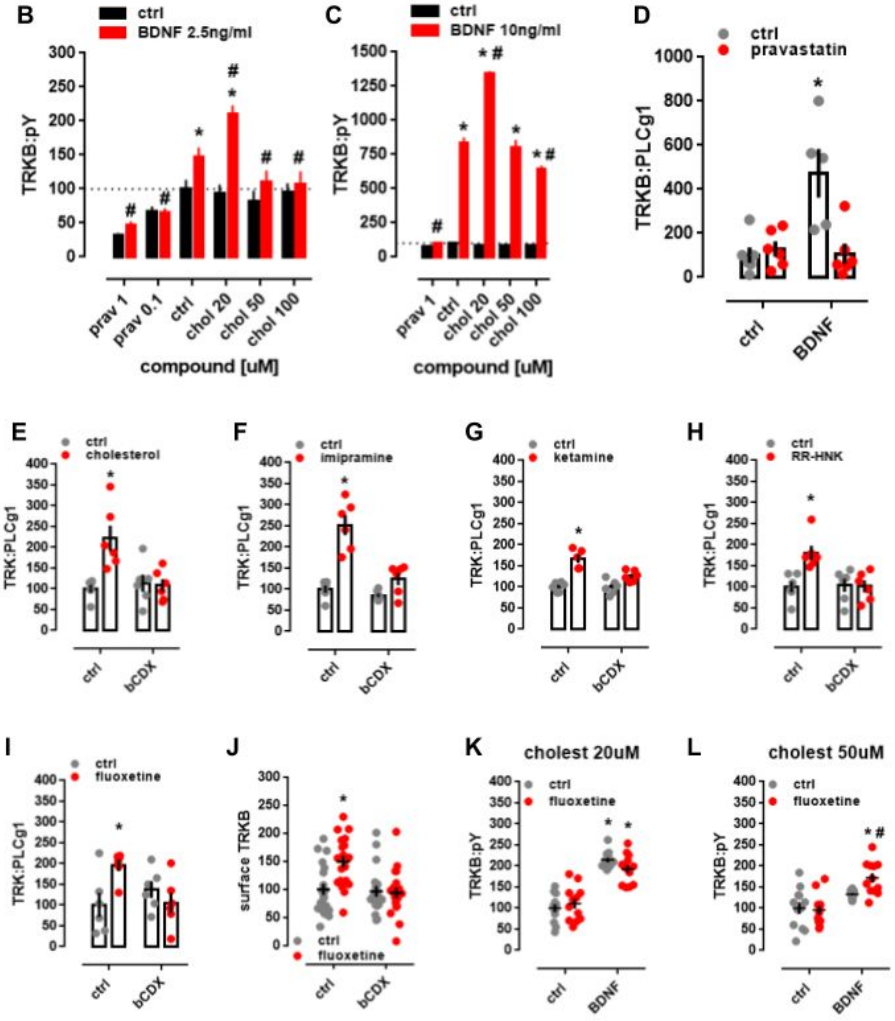

Figure 1. Identification of cholesterol-interacting motif (CARC) in TRKB. (A) Identification of cholesterol-interacting motif (red) in TRKB (NTRK2), but not in TRKA or C (NTRK1 and NTRK3, respectively) transmembrane region. Bold-italicized sequence refers to transmembrane domain. (B) Dual effect of cholesterol in BDNF-induced activation of TRKB [interaction: $F(5,84)=5.654$, $p=0.0002$]. Cholesterol at 20μM facilitates BDNF-induced (2.5ng/ml/15min) TRKB activation, while it's depletion by pravastatin (1μM/3days) or higher doses of cholesterol (50-100μM/30min) reduce it. (C) A similar dual effect of cholesterol on TRKB phosphorylation is also seen at higher concentrations of BDNF (10ng/ml/15min) [interaction: $F(5,84)=5.654$, $p=0.0002$]. The treatment with pravastatin prevented the (D) BDNF-induced (10ng/ml/15min) TRKB:PLC-γ1 coupling [interaction: $F(1,19)=11.23$, $p=0.003$]. *$p<0.05$ from ctrl/ctrl group; #$p<0.05$ from ctrl/BDNF group (Fisher's LSD, n= 6-8/group). (E-I) Cholesterol (20μM/15min) and several antidepressant drugs (10μM/15min) increase TRKB:PLC-γ1 coupling in cortical neurons, and this effect is blocked by βCDX [interaction: cholesterol $F(1,20)=9.608$, $p=0.006$; imipramine $F(1,20)=14.71$, $p=0.001$; ketamine $F(1,19)=9.335$, $p=0.006$; RR-HNK $F(1,20)=8.033$, $p=0.01$; fluoxetine $F(1,20)=8.034$, $p=0.01$]. (J) Fluoxetine increases cell surface exposure of TRKB, and this effect is prevented by βCDX [$F(1,73)=7.022$, $p=0.0099$]. (K) Fluoxetine alone or added together with BDNF (2.5ng/ml/15min) does not facilitate TRKB activation under lower doses of cholesterol (30min) [interaction: $F(1,44)=2.806$, $p=0.1010$], but (L) recovers BDNF effects lost under high doses of cholesterol (30min) [interaction: $F(1,44)=4.335$, $p=0.0432$]. *$p<0.05$ from ctrl/ctrl group; #$p<0.05$ from ctrl/BDNF or ctrl/fluoxetine group (Fisher's LSD). Data expressed as mean/SEM (bars or crosses) of percentage from ctrl/ctrl group (n= 6-20/group).

To investigate the functional effects of TRKB CARC motif, we mutated CARC tyrosine 433 into phenylalanine. Then we evaluated the mobility of GFP-tagged TRKB (WT or Y433F mutant) receptor in neuronal spines using fluorescence recovery after photobleaching (FRAP) assay in transfected hippocampal primary cultures (DIV14). TRKB fluorescence rapidly recovered in neurite shafts after bleaching (figure S2F), however, no recovery was seen in spines. Treatment of neurons with BDNF, fluoxetine or ketamine promoted fluorescence recovery in spines within two minutes (figures S2G and 2A,C). The effects of BDNF and fluoxetine were fully prevented in cells transfected with GFP-tagged TRKB.Y433F (figure 2B,D). Furthermore, BDNF and fluoxetine increased the size of TRKB clusters at the plasma membrane in fibroblasts expressing wild-type TRKB, with attenuated effects in cells expressing TRKB.Y433F, as measured by superresolution microscopy (figure 2E,F). Thus, while the TRKB.Y433F mutation does not change the basal surface localization of TRKB, TRKB translocation to the plasma membrane and clustering in synaptic membranes induced by BDNF (*18*) and antidepressants is dependent on the TRKB CARC domain (figure 2E,F).

.

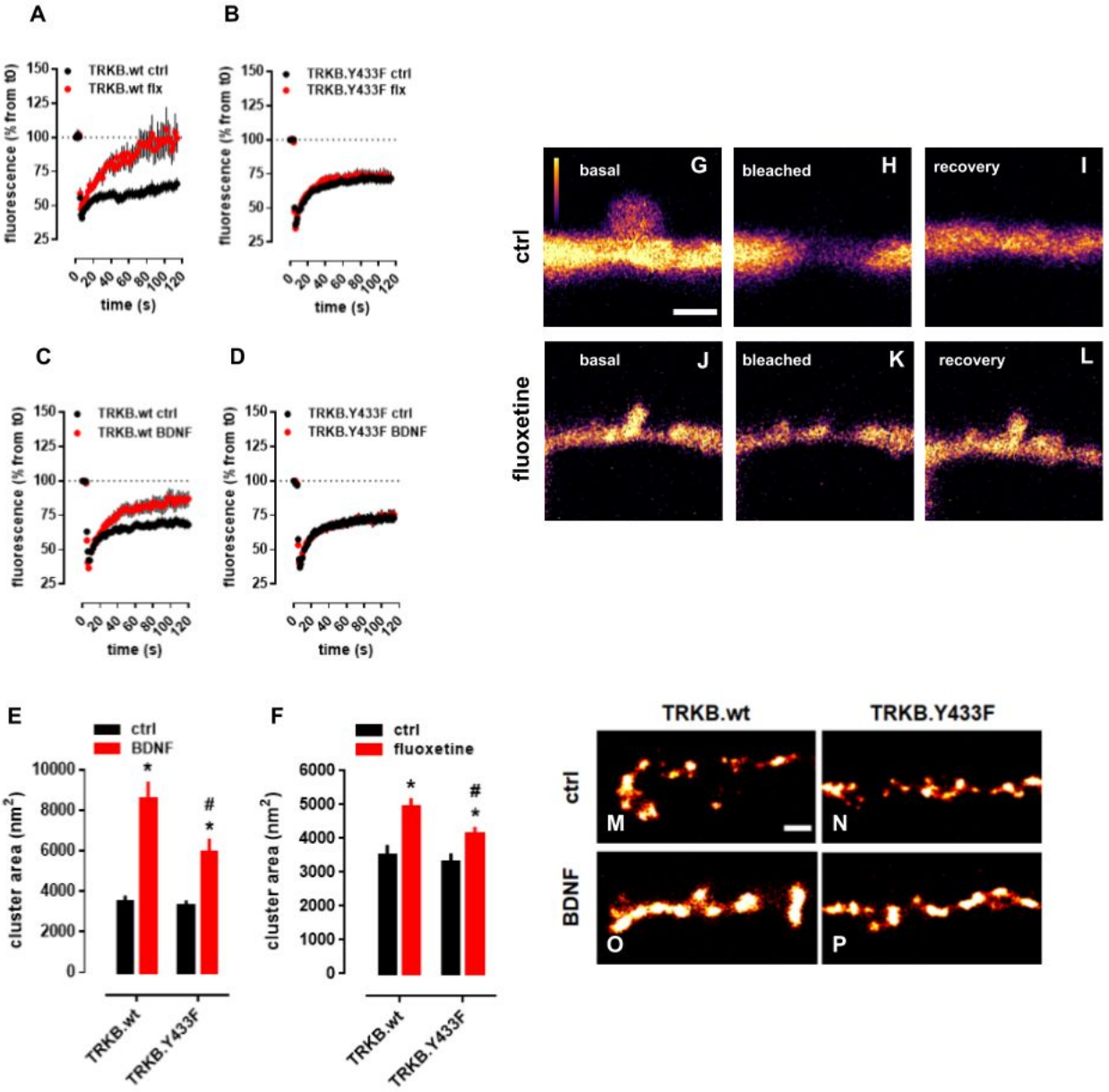

Figure 2. Consequences of TRKB.Y433F mutation in the TRKB turnover and lateral movement. The effect of (A,B) fluoxetine (1μM/15min) or (C,D) BDNF (10ng/ml/15min) triggering the turnover of GFP-tagged TRKB [fluoxetine: $F(177,3068)=2.220$, $p=0.0001$; BDNF: $F(62,2604)=5.435$, $p=0.0001$] in dendritic spines of rat hippocampal neurons (E18; DIV14) is prevented in TRKB.Y433F mutants [fluoxetine: $F(59,4012)=0.5555$, $p=0.99$; BDNF: $F(52,3328)=0.4595$, $p=0.99$], n=9-42/group; mean/SEM of percentage from t=0. The effect of (E) BDNF (10ng/ml/10 min) [$F(1,1677)=72.50$, $p<0.0001$] or (F) fluoxetine (10μM/15min) [$F(1,2122)=18.20$, $p<0.0001$] on the enhanced formation of clusters of GFP-tagged TRKB in the surface of MG87.TRKB cells is attenuated by the TRKB.Y433F mutation. *$p<0.05$ from respective ctrl (vehicle-treated) groups; #$p<0.05$ from BDNF- or fluoxetine-treated wt group (Fisher's LSD), n=232-542 clusters from 10cells/group, and 10 regions of interest (ROI) per picture, mean/SEM of cluster area (squared nm). Representative pictures of the spine and shaft fluorescence in control (G-I) and fluoxetine (J-L) before (basal), immediately (bleached) and 2min (recovery) after photobleaching (for analysis of neurite shaft recovery see figure S2). Scale bar: 1000nm. (M-P) Representative images of the BDNF-induced clusters of TRKB in the surface of MG87.TRKB cells. Scale bar: 250nm.

Atomistic simulations of cholesterol effects on TRKB dimerization

Simulation of TRKB dimerization at transmembrane (TM) helices disclosed five possible structures, but only a cross-like conformation, crossing at the A443-G439 motif, was stable in phosphatidylcholine bilayer with 0 or 20mol% cholesterol (figure 3A,B) (*30*). The Y433 residue (located within CARC motif) stabilizes the structure, and Y433F destabilized it by rotating the TM monomers 40 degrees relative to each other (figure 3D).

Cholesterol binding to the CARC motif was transient (residence times ~100ns or less), and the main factor changing the TM dimer structure was the increase in membrane thickness by cholesterol (figure S5A). In the absence of cholesterol (0mol%), the distance between the TRKB TM C-termini was about 2.2 nm but at 40 mol% the dimer switched from the cross-like to a more parallel conformation (distance ~1.5 nm, figure 3C and S5A). This is consistent with our experimental data suggesting an optimal cholesterol concentration for TRKB function, with a compromised function at low cholesterol concentrations, where the large distance between the C-termini (figure S5B) likely disrupts the conformation of the TRKB ectodomain, and at high concentrations, where the cross-shaped structure is replaced with a presumably unstable more parallel orientation (figure 3D and S5B).

We next simulated the effects of fluoxetine on TRKB.TM structure. Neutral fluoxetine was docked separately to each of the four crevices created by the TRKB dimer through 30 different protein conformations in 1 μs-long molecular dynamics sampling in 20mol% cholesterol membrane. The best scoring configurations consistently featured fluoxetine binding to the crevice facing the extracellular site (figure S6C,D). Only one of the subsequent 120 molecular dynamics simulations (by repositioning the drug around the binding pocket), resulted in a long-lasting stable association overlapping the CARC motif (figure 3E), and recruiting phospholipids to further stabilize binding (figure 3F).

Twenty independent simulations starting from an equilibrated stable protein-fluoxetine complex showed that the Y433F mutation significantly reduced the residence-time of fluoxetine in TRKB homodimers (161ns and >696ns for the mutant and wild-type forms, respectively), indicating that the mutant protein cannot form a stable binding pocket. The data suggest that fluoxetine binding to the dimeric interface acts as a wedge stabilizing the cross-shaped active conformation at high cholesterol concentration. Indeed, in the presence of fluoxetine, the wild-type dimer retains the active state at 40mol% of cholesterol that is close to the one observed in 20mol% cholesterol, maintaining the separation between the C-termini, which is consistent with our biochemical observations (figure 1L). Following drug expulsion, the simulations invariably capture transitioning to the conformation seen in figure 3C.

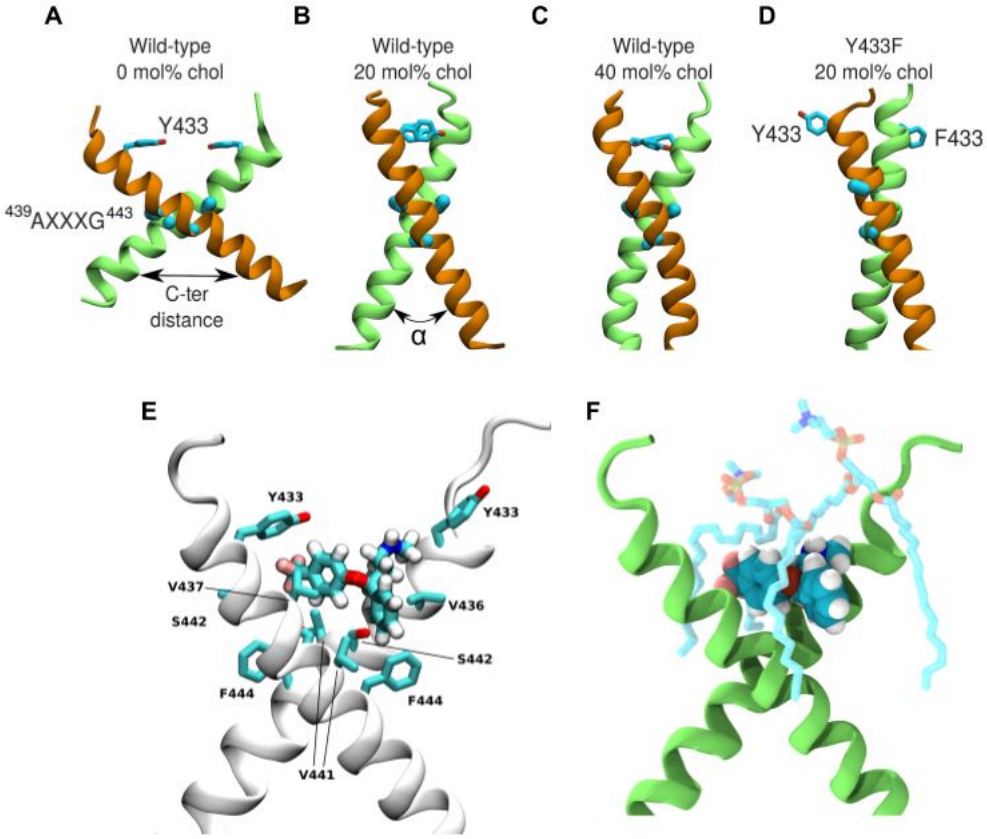

Figure 3. Transmembrane dimer structures for TRKB revealed by atomistic molecular dynamics simulation. (A-C) Structures for wild-type TRKB at cholesterol concentrations of 0 mol%, 20 mol% and 40 mol%, and (D) for the TRKB.wt and TRKB.Y433F heterodimer at 20 mol% (systems 1-4, Table S1, figure S5 for distance and α values between C-termini). (E) Representation of fluoxetine binding to the pocket formed by dimerization of TRKB transmembrane domain. In the wild-type the helices interact via this dimerization motif (A439-G443), while in the case of the Y433F mutant the interface is broken as the mutation enforces the monomers to rotate with respect to one another. (F) The interaction between fluoxetine and TRKB dimer is stabilized by membrane lipids, in this case phosphatidylcholine.

Antidepressant drugs bind to TRKB-cholesterol interaction site

To evaluate the interaction between antidepressants and TRKB we assayed for binding of biotinylated drugs to immunoprecipitated TRKB (*31*). Labeled imipramine, fluoxetine and RR-HNK bound to TRKB with around 3μM affinity (Kd Mean±SEM: imipramine= 2.21±0.79; fluoxetine=3.03±1.34; RR-HNK=1.43±0.46μM). Although imipramine and fluoxetine bind to serotonin transporter (5HTT) with orders of magnitude higher than for TRKB, this affinity corresponds well with concentrations reached in human brain during chronic treatment (*32*, *33*). The same compounds showed significantly lower affinity when assayed with TRKB.Y433F (figure 4A-C). All antidepressants tested displaced labeled imipramine (10μM) binding, with variable efficacy, from 100% for fluoxetine, to 75% and 50% for RR-HNK and ketamine, respectively (figure 4D,E). However, BDNF was completely ineffective in displacing imipramine from TRKB (figure 4F),

and so were 2S,6S-HNK, isoproterenol and aspirin, while chlorpromazine and diphenhydramine produced weak displacement only at 100μM concentrations (figure S2C-E). Cholesterol promoted fluoxetine and RR-HNK (10μM) binding to TRKB with maximal effect achieved at 1μM of added cholesterol (figure 4G,H). TRKB.Y433F mutation attenuated the effect of cholesterol on promoting fluoxetine binding (figure 4I), but this mutation has no effect on the binding of BDNF to TRKB, which takes place at the affinity of 5.7pM (0.08ng/ml; figure 4J). These results suggest that all the investigated antidepressants, at clinically meaningful concentrations (*32*, *33*), bind to TRKB CARC motif. Overall, these results suggest a model where fluoxetine stabilizes the active cross-like conformation, thus delaying the inactivation of TRKB signaling in high cholesterol compartments, and membrane lipids act as a 'lock' to maintain the drug-protein interaction.

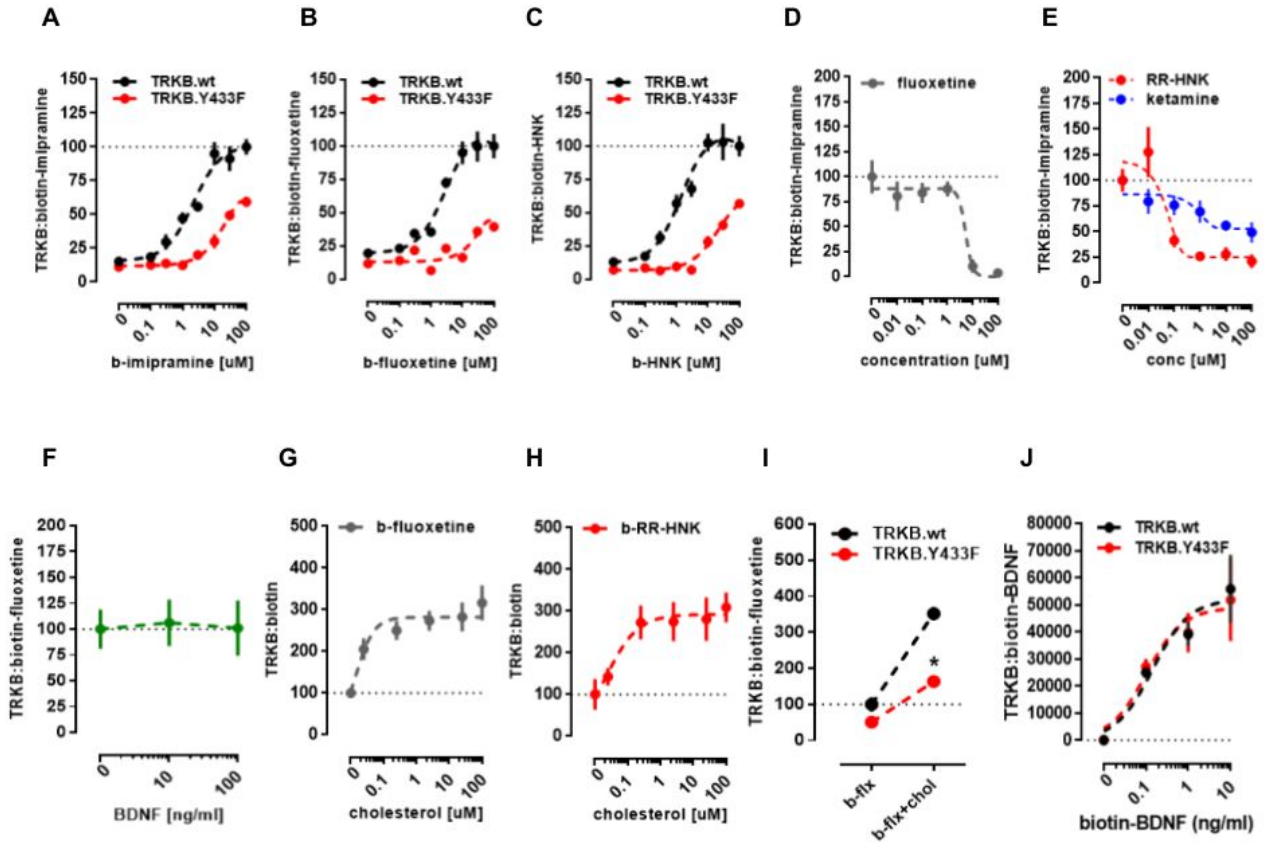

Figure 4. Interaction of antidepressants with TRKB TM domain. (A) Association of biotinylated imipramine [interaction: F(7,160)=14.05, p<0.0001], (B) fluoxetine [interaction: F(7,136)=17.03, p<0.0001], and (C) RR.HNK [interaction: F(7,160)=14.91, p<0.0001] with precipitated TRKB.wt or TRKB.Y433F. Data expressed as percentage from the 100μM group. (D,E) Fluoxetine, ketamine and RR-HNK displace biotinylated imipramine (10μM) from precipitated TRKB.wt (Hill slope: fluoxetine= -3.11; ketamine= -0.06; RR-HNK= -0.59). (F) BDNF does not displace biotinylated fluoxetine from TRKB.wt. Cholesterol increases the interaction between biotinylated (G) fluoxetine or (H) RR-HNK with TRKB.wt (Hill slope: fluoxetine= 25.39; RR-HNK= 6.17), and (I) this effect is reduced in TRKB.Y433F mutats [F(1,71)=18.29, p=0.0001]. (J) The TRKB.Y433F mutation does not change the BDNF interaction with TRKB [F (3, 40) = 0.057, p=0.9818]. *p<0.05 from TRKB.wt in the same condition (Fisher's LSD). Data expressed Mean/SEM of percentage from ctrl/ctrl group (0μM or b-flx, n= 6-14/group).

Cholesterol-TRKB interaction in drug-induced plasticity

BDNF signaling through TRKB is required for LTP, thus we tested whether this effect depends on cholesterol. Infusion of BDNF into the dentate gyrus of anesthetized rats significantly increased synaptic strength, as previously reported (*34*, *35*). However, this effect of BDNF was partially prevented when rats were co-treated with pravastatin (10 mg/kg/day for two weeks; figure 5A). To investigate whether this effect of BDNF on LTP involves TRKB CARC motif, we generated a mouse carrying the TRKB.Y433F mutation. Theta-burst stimulation of hippocampal slices from wild-type mice induced a robust LTP in the CA3-CA1 synapse. Remarkably, stimulation of heterozygous TRKB.Y433F mice failed to induce any potentiation (figure 5B), indicating that TRKB CARC motif is critical for LTP. However, tetanic stimulation induced LTP in both WT and TRKB.Y433F slices (figure S3A-C), consistent with the central role of BDNF role particularly in theta-burst mediated LTP (*36*).

We investigated whether interaction of TRKB and cholesterol plays a role in the learning and memory using object location memory (OLM) test (*37*). Fluoxetine (15mg/kg) and RR-HNK (10mg/kg) significantly improved the OLM test score, and pravastatin (10mg/kg) completely blocked the effects of both drugs (figure 5C,D). Similarly, the improved performance under fluoxetine was blocked in heterozygous TRKB.Y433F (figure 5E) and in the BDNF haploinsufficient mice (figure 5G,H). Remarkably, the serotonin transporter knockout (5HTT.ko) mice, which completely lack the primary site of action of SSRIs, respond to fluoxetine in the same way as the wild-type mice, and pravastatin blocked this effect in both SERT.ko and wild-type mice (figure 5F). This is consistent with the recent finding that the behavioral and electrophysiological effects of SSRIs are preserved in 5HTT.ko mice (*38*). Furthermore, in the contextual fear conditioning paradigm, fluoxetine facilitated extinction of the freezing response, and this effect was lost by co-administration of pravastatin (figure 5I), and in the heterozygous TRKB.Y433F mice (figure 5J).

Fluoxetine treatment reactivates a critical period-like plasticity in the visual cortex of adult rodents (*39*, *40*) and this effect is associated with TRKB activation (*39*). We now observe that RR-HNK induces a similar but faster effect. Remarkably, co-administration of pravastatin attenuates the ocular dominance switch in the visual cortex induced by fluoxetine or RR-HNK (figure 5K,L). Similarly, the effects of fluoxetine on OD plasticity were lost in TRKB.Y433F heterozygous mice (figure 5M).

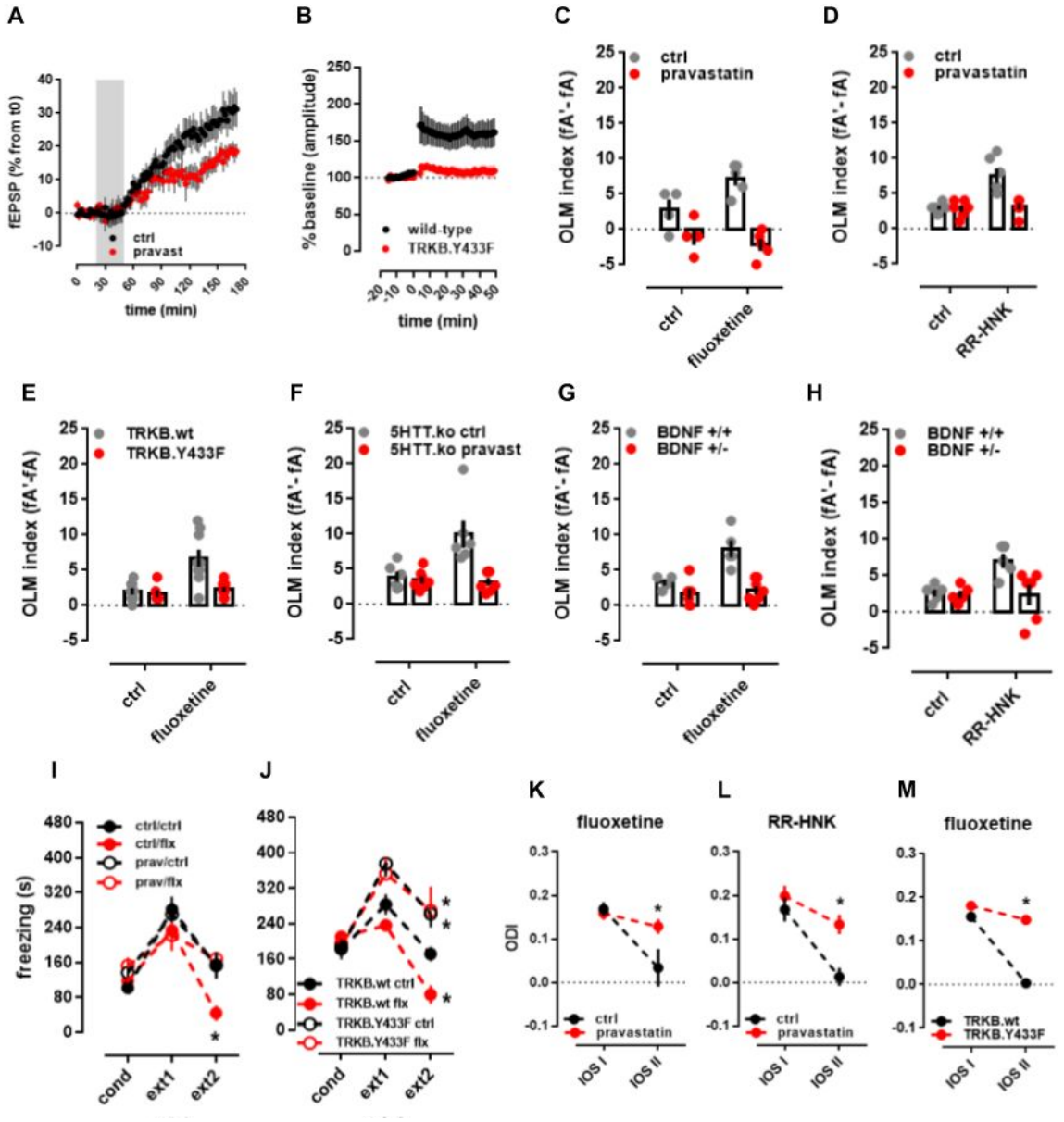

Figure 5. Cholesterol-TRKB interaction induces plasticity. (A) BDNF infusion induced LTP in the dentate gyrus of rats, but pravastatin (10mg/kg/day for 14 days) decreased this effect [interaction: F(85,1290)=1.484; p=0.0036], grey vertical bar: BDNF infusion time (30min; 1microg/ul, at 0.067microl/min rate). (B) Theta-burst induced LTP in the CA3-CA1 synapses of hippocampal slices from wild-type mice, but this effect was absent in slices from Y433F mutant mice [interaction F(61,620)=1.657, p=0.0019]; mean/SEM from baseline [in A t=0; in B t= -20min]. In OLM task, (C) fluoxetine (15mg/kg/day for 7days) [interaction: F(1,14)=6.504, p=0.023] and (D) RR-HNK (10mg/kg/day for 3 days) [interaction: F(1,20)=10.59, p=0.004] improved object location memory in wild-type mice, but this effect was prevented by pravastatin (10mg/kg/day) and (E) absent in the TRKB.Y433F mutant mice [interaction: F(1,27)=6.520, p=0.016]. (F) The effects of fluoxetine on OLM are retained in the 5HTT (SERT) knockout animals and blocked by pravastatin [interaction: F(1,22)=9.632, p=0.0052]. The effect of (G) fluoxetine [interaction: F(1,18)=6.878, p=0.017] and (H) RR-HNK [interaction: F(1,17)=5.042, p=0.003] are lost in BDNF haploinsufficient (+/-) mice. Data expressed as mean/SEM (black crosses) of OLM index (difference in the number of visits to the new - A' and old - A objects), n=4-10/group. (I) Fluoxetine facilitated the extinction of contextual conditioned fear, and this response is blocked by pravastatin [interaction: F(6,40)=5.099, p=0.0006]; (J) a similar effect was observed in mice carrying the TRKB.Y433F mutation [interaction: F(6,34)=3.241, p=0.0126]. *p<0.05 from ctrl/ctrl or ctrl/wt group in the same session (Fisher's LSD), mean/SEM of total freezing time in the 8 min session, n=5-6/group. (K-L) Treatment with fluoxetine (10mg/kg/day for 28 days) or RR-HNK (10mg/kg every 2 days, for 7 days) induces a shift in ocular dominance in response to 7 days of monocular deprivation, but this effect is prevented by a simultaneous pravastatin treatment [fluoxetine/ctrl vs fluoxetine/pravastatin in IOS II: p=0.0454; RR-HNK/ctrl vs RR-HNK/pravastatin in IOS II: p=0.0031, Fisher's LSD]. (E) Fluoxetine fails to induce a shift in ocular dominance in TRKB.Y433F mice [interaction: F(1,11)=48.70, p<0.0001]. *p<0.05 from vehicle-treated group in the same session (Fisher's LSD), mean/SEM of ocular dominance index (ODI), n=4-7/group.

Discussion

Here we demonstrate that cholesterol prolongs TRKB surface expression and BDNF signaling, which provides a mechanism for the essential role of cholesterol in neuronal maturation and synaptic transmission (*20*, *21*). Cholesterol plays a permissive role in BDNF-induced TRKB activation, but high cholesterol concentrations limit BDNF signaling, which agrees with previous studies showing that TRKB predominantly resides outside lipid rafts but can transiently signal in these domains (*18*, *41*). Pravastatin and TRKB.Y433F mutation inhibit BDNF and theta-burst-induced LTP, respectively, and prevent antidepressant-induced learning and ocular dominance plasticity. Our findings indicate that TRKB may be the critical target through which astrocyte-derived cholesterol promotes synaptic function and plasticity (*20*, *21*).

BDNF signaling is crucial to the action of essentially all antidepressant drugs, but this effect has been assumed to be indirect, through other molecules such as 5HTT or NMDA receptors. We now show that antidepressants bind to the transmembrane region of TRKB dimers with a therapeutically relevant affinity (*33*), favoring translocation of TRKB to plasma membrane, where it is accessible to BDNF. This binding is shared by typical tricyclic and SSRI antidepressants, as well as by the rapid-acting ketamine and its metabolite RR-HNK. Mutagenesis demonstrates the critical role of the TRKB CARC motif as the binding site for antidepressants. Simulation data reveals that antidepressants stabilize TRKB dimers in a BDNF-activatable conformation that is stable in synaptic membranes with high cholesterol concentrations. The affinity to TRKB is comparable to the affinity of ketamine to NMDA receptors but low when compared to the affinity of SSRIs to serotonin transporter. However, 5HTT does not seem to mediate the behavioral effects of SSRIs [(*38*), figure 5F] and micromolar concentrations of SSRIs are reached in the brain during chronic treatment (*32*, *33*). The gradual brain accumulation of concentration needed for TRKB binding might be at least one reason why typical antidepressants take so long to act, while the rapid brain penetration of ketamine and HNK enables fast action.

Our findings that antidepressants bind to TRKB and thereby prolong BDNF signaling directly links the effects of these drugs to neuronal plasticity (*8*, *39*, *42*). Juvenile-like plasticity induced by antidepressants in the adult brain facilitates beneficial re-adaptation of neuronal networks abnormally wired during development or stress, which may explain the superiority of the antidepressant and psychotherapy combination (*43*). Our data suggests a new framework for the antidepressant action where the drugs bind to the cholesterol-interaction site of TRKB thereby prolonging BDNF-induced plasticity that is permissive for the activity-dependent network rewiring underlying the clinical antidepressant response.

Methods

Protein-protein and ligand docking: For simulations, the secondary structure prediction and modeling of the transmembrane domain of TRKB (residues 427-459) were performed using the FMAP (Folding of Membrane-Associated Peptides) server (*44*). The initial models of the TRKB transmembrane (TM) (amino acids 427-459) dimers for atomistic MD simulations were generated using the MPDock application of the Rosetta software suite (*45*). The drug-binding pocket was characterized by local docking of the drugs to the TRKB TM dimers using the RosettaScripts interface (*46*).

Molecular Dynamics simulations. All atomistic simulations were performed using Gromacs 2018 (*47*) employing the Charmm36(m) force field for the protein (*48*) and lipids (*49*), TIP3P water model (*50*), and a compatible ion parameter set (*51*). Drug parameters were generated using the CHARMM General Force Field (CGenFF) program (*52*). Lipid membranes were comprised of POPC with a varying concentration of cholesterol (0, 20, 40 mol%). All production simulations were performed in the NpT ensemble at a pressure of 1 bar at three different temperatures (310 K, 333 K, 363 K); key data and conclusions are based on 310 K. All protein-membrane systems were constructed using CHARMM-GUI (*53*), and all simulation parameters were chosen as suggested.

Free energy calculations. All free energy calculations were performed using the free energy perturbation (FEP) method with Hamiltonian replica exchange. The free energies and their statistical errors were estimated with the Multistate Bennett Acceptance Ratio (MBAR) method using the Alchemical Analysis and the pymbar software (*54*). The necessary corrections arising due to the added restraints and the decoupled intra-molecular interactions were applied to obtain the final free energy values.

Analysis. All simulations were repeated through several replicas and the total simulation time covering all simulations was >500 microseconds. All analyses of these data were performed using the tools available in Gromacs 2018 and VMD (*55*), together with in-house scripts and software. A detailed description of simulation systems and parameters is given in supplement file.

Animals: adult male rats were used for *in vivo* BDNF-induced LTP. Adult male and female mice (12-20 weeks): BDNF haploinsufficient, SERT.ko, TRKB.Y433F.het, with respective wild-type littermates, were used in object-location memory, contextual fear conditioning or ocular dominance plasticity. All animals were kept group housed with free access to food and water, except during the experimental sessions. All protocols were approved by local ethical committees (Finland: ESAVI/10300/04.10.07/2016; Norway: 6159; Germany: G-18-88).

Drugs and reagents: cholesterol, beta-cyclodextrin, pravastatin, fluoxetine, imipramine, ketamine, 2R,6R-HNK (RR-HNK), 2S,6S-HNK, aspirin, chlorpromazine, isoproterenol, diphenhydramine, BDNF, and NGF. The amino-biotinylation of fluoxetine, RR-HNK and imipramine was performed using a commercial kit (EZ-Link NHS-PEG4 Biotinylation Kit, #21455, Thermo Scientific). Antibodies: TRKB (R&D, #AF1494); PLC-γ1 (CST, #5690); pY (AbD Serotec, #MCA2472B); actin (#sc1615); GFP (#ab290, Abcam); HRP-conj anti-Gt IgG (Invitrogen, #61-1620), anti-Rb IgG (BioRad, #170-5046); HRP-conj streptavidin (Thermo Fisher, #21126).

Cell culture and transfections: HEK293T (used for production of GFP-tagged TRKB), MG87.TRKB cells and primary cultures of E18 rat embryos (DIV8 for biochemical analysis and DIV14 for FRAP) were cultivated according to previously described protocols (*56*–*58*). The cells were transfected (DIV13 for hippocampal neurons) to express GFP-tagged TRKB (wt or Y433F) using lipofectamine 2000, according to manufacturer's instructions (#11668019, Thermo Fisher) 24h prior the experimental sessions or sample collection.

ELISA: the TRKb:pY (pTRKB), TRKB:PLC-γ1 interaction, the levels of phosphorylated TRKB and surface TRKB were measured by ELISA (*57*, *58*).

Cell viability: the cell viability was determined using CellTiterGlo kit according to the manufacturer's instructions (#G7571; Promega).

Drug binding assay: the drug/BDNF interaction with TRKB was determined by ELISA based on literature (*31*). TRKB.wt or TRKB.Y433F were expressed in HEK293T cells, and immunoprecipitated in 96-well plates. Increasing doses of biotinylated drugs (0.1-100μM) or BDNF (0.1-100ng/ml) were added after blocking with 2% BSA in PBS for 1h and the signal developed by incubation with HRP-conjugated streptavidin followed by ECL. For the competitive assay, increased doses of non-biotinylated drugs (0.001-100μM) or BDNF (10-100ng/ml) were mixed with 10μM of biotinylated imipramine or fluoxetine for 1h, and the signal developed as described. Cholesterol (0.1-100μM) was incubated with 10μM of biotinylated fluoxetine or RR-HNK for 1h, and the signal developed as described.

FRAP: hippocampal cells from E18 rat embryos (DIV14) were transfected to express GFP-TRKB.wt or GFP-TRKB.Y433F. Upon identification of GFP-positive cells, the whole spine head or the neurite shaft was bleached with high laser power (*59*) and the latency for fluorescence recovery was quantified.

TIRF/dSTORM: MG87.TRKB cells were transfected to also express GFP-TRKB.wt or GFP-TRKB.Y433F prior to immunostaining for GFP, and the area of GFP-tagged TRKB cell surface clusters was determined by total internal reflection fluorescence microscopy (TIRF) coupled with direct stochastic optical reconstruction microscopy (dSTORM).

Immunostaining and Sholl analysis: cortical cells (E18 rat embryo, DIV8) were fixed and labeled for actin. The number of intersections from the cell body was counted using FIJI plug-in (*60*).

Electrophysiology: in vivo and ex vivo
In vivo BDNF-induced LTP was performed according to literature (*34*, *35*).
Ex vivo activity-induced LTP: TBS and tetanus stimulus was performed according to literature (*61*).

Ocular dominance plasticity assay:
The shift in ocular dominance induced by drug treatment was performed according to literature (*40*), workflow can be found in figure S4C.

Behavioral analysis:
OLM: the animals were trained for 15min session, during 3 days in a square arena containing cues in the walls, with two identical objects. In the test session, one of the objects is moved to a different position, and the number of visits during the 5min session to each (old- and newly-positioned) object is counted.
Fear conditioning: the animals received 5 scrambled foot shocks (0.6mA/2s) in an 8 min conditioning session. The animals were exposed to the same context in two extinction sessions (separated by 24h interval) and the time spent in freezing was automatically determined (TSE systems). Workflow for OLM and fear conditioning can be found in figure S4A,B.

Statistics: one- or two-way ANOVA were used, followed by Fisher's LSD *post hoc* test. *F* and *p* values are indicated in the figure legends.

Acknowledgements: The authors would like to thank Sulo Kolehmainen and Seija Lågas (Neuroscience Center - UH), and the Biomedicum Imaging Unit (BIU) at the University of Helsinki for technical help. We also thank Dr. Todd Gould (U. of Maryland) and Dr. Craig Thomas (NIH) for kindly supplying the RR-HNK used in this study, profs. Yves-Alain Barde, Maija Castrén, Heikki Ruskoaho and Mart Saarma for their insightful comments to the present manuscript.

Funding: work in Castrén lab was supported by the ERC grant #322742 - iPLASTICITY; EU Joint Programme - Neurodegenerative Disease Research (JPND) CircProt project #301225, Sigrid Jusélius Foundation, Jane and Aatos Erkko Foundation, and the Academy of Finland grants #294710 and #307416. Work in Bramham lab was supported by the EU Joint Programme - Neurodegenerative Disease Research (JPND) CircProt project #30122. Work in Lauri lab was funded by the Academy of Finland grant #297211. Work in Vattulainen group was supported by the Academy of Finland (Center of Excellence) #307415, Sigrid Juselius Foundation, Helsinki Institute of Life Science, and CSC - IT Center for Science (computing resources). The work in Normann and Serchov lab was funded by the German Research Council (#SE 2666/2-1) and the Forschungskommission of the Medical Faculty of the University of Freiburg (#SER1149/17). None of the funders had a role in the data acquisition and analysis, or manuscript preparation.

Authors contributions: PCC, CB, IV and EC designed the experiments; PCC, SMF and CB performed the biochemical experiments with the assistance of LL and IC. MG, GE, TR and IV performed the molecular modeling and simulation experiments. RM and CAB performed the imaging experiments; CC, HA and AS performed intrinsic optical imaging experiments; FW, SP, and SL performed the electrophysiology experiments. PCC, SV, and TS performed the behavioral studies; PCC and EC wrote the manuscript, with the help of MG, TR, CRB, CN and IV.

Competing interests: the authors declare no competing interests.

References

1. R. H. Belmaker, G. Agam, Major depressive disorder. *N. Engl. J. Med.* **358**, 55–68 (2008).
2. C. A. Zarate Jr *et al.*, A randomized trial of an N-methyl-D-aspartate antagonist in treatment-resistant major depression. *Arch. Gen. Psychiatry*. **63**, 856–864 (2006).
3. C. G. Abdallah, G. Sanacora, R. S. Duman, J. H. Krystal, Ketamine and rapid-acting antidepressants: a window into a new neurobiology for mood disorder therapeutics. *Annu. Rev. Med.* **66**, 509–523 (2015).
4. P. Zanos *et al.*, NMDAR inhibition-independent antidepressant actions of ketamine metabolites. *Nature*. **533**, 481–486 (2016).
5. E. W. Lumsden *et al.*, Antidepressant-relevant concentrations of the ketamine metabolite (2R,6R)-hydroxynorketamine do not block NMDA receptor function. *Proc. Natl. Acad. Sci. U. S. A.* **116**, 5160–5169 (2019).
6. R. S. Duman, G. R. Heninger, E. J. Nestler, A molecular and cellular theory of depression. *Arch. Gen. Psychiatry*. **54**, 597–606 (1997).
7. A. E. Autry, L. M. Monteggia, Brain-derived neurotrophic factor and neuropsychiatric disorders. *Pharmacol. Rev.* **64**, 238–258 (2012).
8. E. Castrén, H. Antila, Neuronal plasticity and neurotrophic factors in drug responses. *Mol. Psychiatry* (2017), doi:10.1038/mp.2017.61.
9. T. Saarelainen *et al.*, Activation of the TrkB neurotrophin receptor is induced by antidepressant drugs and is required for antidepressant-induced behavioral effects. *J. Neurosci.* **23**, 349–357 (2003).
10. T. Rantamäki *et al.*, Pharmacologically diverse antidepressants rapidly activate brain-derived neurotrophic factor receptor TrkB and induce phospholipase-Cgamma signaling pathways in mouse brain. *Neuropsychopharmacology*. **32**, 2152–2162 (2007).
11. H. Thoenen, Neurotrophins and neuronal plasticity. *Science*. **270**, 593–598 (1995).
12. H. Park, M.-M. Poo, Neurotrophin regulation of neural circuit development and function. *Nat. Rev. Neurosci.* **14**, 7–23 (2013).
13. Y. Lu, K. Christian, B. Lu, BDNF: a key regulator for protein synthesis-dependent LTP and long-term memory? *Neurobiol. Learn. Mem.* **89**, 312–323 (2008).
14. M. V. Chao, Neurotrophins and their receptors: a convergence point for many signalling pathways. *Nat. Rev. Neurosci.* **4**, 299–309 (2003).
15. E. Castrén, Neuronal network plasticity and recovery from depression. *JAMA Psychiatry*. **70**, 983–989 (2013).
16. S. Suzuki *et al.*, Brain-Derived Neurotrophic Factor Regulates Cholesterol Metabolism for Synapse Development. *Journal of Neuroscience*. **27**, 6417–6427 (2007).
17. B. Zonta, L. Minichiello, Synaptic membrane rafts: traffic lights for local neurotrophin signaling? *Front. Synaptic Neurosci.* **5** (2013), doi:10.3389/fnsyn.2013.00009.
18. S. Suzuki *et al.*, BDNF-induced recruitment of TrkB receptor into neuronal lipid rafts: roles in synaptic modulation. *J. Cell Biol.* **167**, 1205–1215 (2004).
19. M. G. Martin *et al.*, Cholesterol Loss Enhances TrkB Signaling in Hippocampal Neurons Aging in Vitro. *Mol. Biol. Cell*. **19**, 2101–2112 (2008).
20. D. H. Mauch, CNS Synaptogenesis Promoted by Glia-Derived Cholesterol. *Science*. **294**, 1354–1357 (2001).
21. M. G. Martin *et al.*, Constitutive hippocampal cholesterol loss underlies poor cognition in old rodents. *EMBO Mol. Med.* **6**, 902–917 (2014).
22. E. Ikonen, Cellular cholesterol trafficking and compartmentalization. *Nat. Rev. Mol. Cell Biol.* **9**, 125–138 (2008).
23. K. Tulodziecka *et al.*, Remodeling of the postsynaptic plasma membrane during neural development. *Mol. Biol. Cell*. **27**, 3480–3489 (2016).
24. A. Di Lieto *et al.*, The responsiveness of TrkB to BDNF and antidepressant drugs is differentially regulated during mouse development. *PLoS One*. **7**, e32869 (2012).
25. J. Chen, D. Korostyshevsky, S. Lee, E. O. Perlstein, Accumulation of an antidepressant in vesiculogenic membranes of yeast cells triggers autophagy. *PLoS One*. **7**, e34024 (2012).
26. Z. Xia *et al.*, Antidepressant-induced lipidosis with special reference to tricyclic compounds. *Prog. Neurobiol.* **60**, 501–512 (2000).
27. S. J. Erb, J. M. Schappi, M. M. Rasenick, Antidepressants Accumulate in Lipid Rafts Independent of Monoamine Transporters to Modulate Redistribution of the G Protein, Gαs. *J. Biol. Chem.* **291**, 19725–19733 (2016).
28. N. H. Wray, J. M. Schappi, H. Singh, N. B. Senese, M. M. Rasenick, NMDAR-independent, cAMP-dependent antidepressant actions of ketamine. *Mol. Psychiatry* (2018), doi:10.1038/s41380-018-0083-8.
29. J. Fantini, F. J. Barrantes, How cholesterol interacts with membrane proteins: an exploration of cholesterol-binding sites including CRAC, CARC, and tilted domains. *Front. Physiol.* **4** (2013), doi:10.3389/fphys.2013.00031.
30. J. K. L. Sinclair, A. S. Walker, A. E. Doerner, A. Schepartz, Mechanism of Allosteric Coupling into and through the Plasma Membrane by EGFR. *Cell Chem Biol.* **25**, 857–870.e7 (2018).
31. I. Das *et al.*, Preventing proteostasis diseases by selective inhibition of a phosphatase regulatory subunit. *Science*. **348**, 239–242 (2015).
32. N. R. Bolo *et al.*, Brain pharmacokinetics and tissue distribution in vivo of fluvoxamine and fluoxetine by fluorine magnetic resonance spectroscopy. *Neuropsychopharmacology*. **23**, 428–438 (2000).
33. C. N. Karson *et al.*, Human brain fluoxetine concentrations. *J. Neuropsychiatry Clin. Neurosci.* **5**, 322–329 (1993).
34. E. Messaoudi, K. Bårdsen, B. Srebro, C. R. Bramham, Acute intrahippocampal infusion of BDNF induces lasting potentiation of synaptic transmission in the rat dentate gyrus. *J. Neurophysiol.* **79**, 496–499 (1998).
35. D. Panja, C. R. Bramham, BDNF mechanisms in late LTP formation: A synthesis and breakdown. *Neuropharmacology*. **76 Pt C**, 664–676 (2014).
36. L. Minichiello *et al.*, Mechanism of TrkB-mediated hippocampal long-term potentiation. *Neuron*. **36**, 121–137 (2002).
37. E. Dere, J. P. Huston, M. A. De Souza Silva, The pharmacology, neuroanatomy and neurogenetics of one-trial object recognition in rodents. *Neurosci. Biobehav. Rev.* **31**, 673–704 (2007).
38. C. Normann *et al.*, Antidepressants Rescue Stress-Induced Disruption of Synaptic Plasticity via Serotonin Transporter-Independent Inhibition of L-Type Calcium Channels. *Biol. Psychiatry*. **84**, 55–64 (2018).
39. J. F. Maya Vetencourt *et al.*, The antidepressant fluoxetine restores plasticity in the adult visual cortex. *Science*. **320**, 385–388 (2008).
40. A. Steinzeig, D. Molotkov, E. Castrén, Chronic imaging through “transparent skull” in mice. *PLoS One*. **12**, e0181788 (2017).

41. D. B. Pereira, M. V. Chao, The tyrosine kinase Fyn determines the localization of TrkB receptors in lipid rafts. *J. Neurosci.* **27**, 4859–4869 (2007).
42. N. N. Karpova *et al.*, Darkness reduces BDNF expression in the visual cortex and induces repressive chromatin remodeling at the BDNF gene in both hippocampus and visual cortex. *Cell. Mol. Neurobiol.* **30**, 1117–1123 (2010).
43. S. Pampallona, P. Bollini, G. Tibaldi, B. Kupelnick, C. Munizza, Combined pharmacotherapy and psychological treatment for depression: a systematic review. *Arch. Gen. Psychiatry*. **61**, 714–719 (2004).
44. A. L. Lomize, J. M. Hage, I. D. Pogozheva, Membranome 2.0: database for proteome-wide profiling of bitopic proteins and their dimers. *Bioinformatics*. **34**, 1061–1062 (2018).
45. R. F. Alford *et al.*, An Integrated Framework Advancing Membrane Protein Modeling and Design. *PLoS Comput. Biol.* **11**, e1004398 (2015).
46. S. J. Fleishman *et al.*, RosettaScripts: a scripting language interface to the Rosetta macromolecular modeling suite. *PLoS One*. **6**, e20161 (2011).
47. M. J. Abraham *et al.*, GROMACS: High performance molecular simulations through multi-level parallelism from laptops to supercomputers. *SoftwareX*. **1-2**, 19–25 (2015).
48. J. Huang *et al.*, CHARMM36m: an improved force field for folded and intrinsically disordered proteins. *Nat. Methods*. **14**, 71–73 (2017).
49. J. B. Klauda *et al.*, Update of the CHARMM all-atom additive force field for lipids: validation on six lipid types. *J. Phys. Chem. B*. **114**, 7830–7843 (2010).
50. W. L. Jorgensen, J. Chandrasekhar, J. D. Madura, R. W. Impey, M. L. Klein, Comparison of simple potential functions for simulating liquid water. *J. Chem. Phys.* **79**, 926–935 (1983).
51. D. Beglov, B. Roux, Finite representation of an infinite bulk system: Solvent boundary potential for computer simulations. *J. Chem. Phys.* **100**, 9050–9063 (1994).
52. K. Vanommeslaeghe *et al.*, CHARMM general force field: A force field for drug-like molecules compatible with the CHARMM all-atom additive biological force fields. *J. Comput. Chem.* **31**, 671–690 (2009).
53. S. Jo, T. Kim, V. G. Iyer, W. Im, CHARMM-GUI: a web-based graphical user interface for CHARMM. *J. Comput. Chem.* **29**, 1859–1865 (2008).
54. P. V. Klimovich, M. R. Shirts, D. L. Mobley, Guidelines for the analysis of free energy calculations. *J. Comput. Aided Mol. Des.* **29**, 397–411 (2015).
55. W. Humphrey, A. Dalke, K. Schulten, VMD: visual molecular dynamics. *J. Mol. Graph.* **14**, 33–8, 27–8 (1996).
56. M. P. Sahu, O. Nikkilä, S. Lågas, S. Kolehmainen, E. Castrén, Culturing primary neurons from rat hippocampus and cortex. *Neuronal Signaling*. **3**, NS20180207 (2019).
57. S. M. Fred *et al.*, Pharmacologically diverse antidepressant drugs disrupt the interaction of BDNF receptor TRKB and the endocytic adaptor AP-2. *bioRxiv* (2019), p. 591909.
58. H. Antila *et al.*, Utilization of in situ ELISA method for examining Trk receptor phosphorylation in cultured cells. *J. Neurosci. Methods*. **222**, 142–146 (2014).
59. M. Koskinen, E. Bertling, P. Hotulainen, Methods to measure actin treadmilling rate in dendritic spines. *Methods Enzymol.* **505**, 47–58 (2012).
60. J. Schindelin *et al.*, Fiji: an open-source platform for biological-image analysis. *Nat. Methods*. **9**, 676–682 (2012).
61. D. Popova, E. Castrén, T. Taira, Chronic fluoxetine administration enhances synaptic plasticity and increases functional dynamics in hippocampal CA3-CA1 synapses. *Neuropharmacology*. **126**, 250–256 (2017).